Optics Communications 478 (2021) 126374

Contents lists available at ScienceDirect

Optics Communications

journal homepage: www.elsevier.com/locate/optcom

Effects of smoothing functions on the transformation of TM to TE propagation problems in the framework of FFT-BPM: A comparative study

Adel Shaaban [a], Yi-Chun Du, Ph.D. [b,c,*], Lotfy Rabeh Gomaa, Ph.D. [d]

[a] Department of Radiation Engineering, National Center for Radiation Research (NCRRT), Atomic Energy Authority, Cairo 11765, Egypt
[b] Department of Biomedical Engineering, National Cheng Kung University, Tainan 70105, Taiwan
[c] Medical Device Innovation Center, National Cheng Kung University, Tainan 70105, Taiwan
[d] Faculty of Engineering at Shobra, Banha University, Cairo 11672, Egypt

ARTICLE INFO

Keywords:
Beam propagation method
Plasmonics
Computational electromagnetics

ABSTRACT

It is well understood that transverse magnetic (TM) polarized optical beams could not be considered by the FFT-BPM because of the presence of the mixed derivatives of the magnetic field and refractive index in the relevant wave equation. Such mixed derivatives could be resolved by transforming the TM problem to an equivalent TE one via an "equivalent refractive index" formalism. Unfortunately, if the refractive index of the original TM problem has step-like discontinuities along the optical confinement direction (transverse to the propagation direction), the "equivalent index" in the transformed TE problem will exhibit a Dirac-delta distribution at the planes of these discontinuities because the "equivalent index" involves second derivative of the inverse of the original refractive index of the TM problem. The Dirac-delta distribution could be eliminated by approximating the step-like original refractive index by a smoothed one, and hence the derivative in the equivalent index could be evaluated analytically as well as numerically; this eliminates the spike-like behavior of the equivalent index at the plane of the discontinuities. In this paper, we present a wide variety of smoothing functions that exist in the literature and assess their effects on the final numerical results of the problem under consideration. The comparative study presented here will help the interested researchers when deciding which smoothing function is appropriate for a specific problem.

1. Introduction

Miniaturized optical component are taking a forefront place in nanotechnology. Unfortunately, the development of such components is impeded by the diffraction limit. Nevertheless, surface plasmonics, tightly bound to the interface between a metal and a dielectric, offer a viable way to circumvent the diffraction limit of optical energy confinement within nanoscale guiding structures and devices [1]. We can say that, surface plasmon-based circuits present a key component able to merge photonics and electronics at the nanoscale. That is, plasmonic waveguides are on the top of light guides that strongly confine optical energy with low propagation losses [2–5]. In fact, the advancement in the field of light manipulation and enhancement on subwavelength scale, relies heavily on the development of powerful design and simulation methods, as well as new characterization techniques. finite difference frequency domain (FDFD) and Finite difference time domain (FDTD) are popular simulation methods used for modeling the plasmonic waveguide [6,7]. The majority of the simulations are focusing on the modal characterization of such waveguide [8]. In this paper we present the FFT-BPM to investigate the sub-wavelength plasmonic structures and configurations. It is well understood that, the excitation of surface plasmon wave must use transverse magnetic (TM) polarized optical beams, which could not be considered by the FFT-BPM in its classical form, because of the presence of the mixed derivatives of the magnetic field and refractive index in the relevant TM wave equation [9]. This could be resolved by transforming the TM problem to an equivalent TE one via an ‘‘equivalent refractive index’’ formalism [9,10]. This eliminates the mixed derivatives in the resulting TE wave equation. However, the equivalent index still involves derivatives of the original step-like refractive index of the waveguide. This introduces a ‘‘spike-like’’ singularity in the equivalent index which prevents its numerical evaluation unless a well-behaved smoothing function is used to approximate the original refractive index. Many functions exist in the literature [3,4,9–11]. An assessment of the behavior of a variety of smoothing functions is presented for comparative purposes.

* Corresponding author at: Department of Biomedical Engineering, National Cheng Kung University, Tainan 70105, Taiwan.
E-mail addresses: engadelsas@gmail.com (A. Shaaban), terrydu@gs.ncku.edu.tw (Y.-C. Du), lotfigomaa@gmail.com (L.R. Gomaa).

https://doi.org/10.1016/j.optcom.2020.126374
Received 7 May 2020; Received in revised form 2 August 2020; Accepted 12 August 2020
Available online 19 August 2020

2. Analytical considerations

Recalling that the wave equation in the TM case for the magnetic field H_y *(x, z)* in a y-invariant structure takes the form:

$$\nabla^2 H_y(x,z) + k_0^2 n^2(x) H_y(x,z) - \frac{1}{n^2(x)} \frac{\partial n^2(x)}{\partial x} \frac{\partial H_y(x,z)}{\partial x} = 0 \quad (1)$$

where, the free space wavevector $k_o = \frac{2\pi}{\lambda}$ and λ is the free space wavelength, $\nabla^2 = \frac{\partial^2}{\partial x^2} + \frac{\partial^2}{\partial z^2}$ and *n(x)* is the refractive index profile of the waveguiding structure. In Eq. (1) the main problem facing the applicability of the traditional FFT-BPM is the third term involving the product of the derivatives of the field and the refractive index profile [9]. Hoekstra et al. [12] and Poladian et al. [13] suggested a transformation of the problem from TM to a TE one via the following simple field transformation:

$$U(x,z) = H_y(x,z)/n(x) \quad (2)$$

Upon substitution of Eq. (2) in Eq. (1), the resulting TE wave equation for *U*(x,z) takes the form:

$$[\nabla^2 + k_o^2 n_{eq}^2(x)]U(x,z) = 0 \quad (3)$$

where the equivalent refractive index is defined as:

$$n_{eq}^2(x) = n^2(x) - \frac{n(x)}{k_o^2} \frac{\partial^2}{\partial x^2}\left(\frac{1}{n(x)}\right) \quad (4)$$

Eq. (4) is now amenable to be evaluated numerically. However, the refractive index profile *n(x)* of the step-index waveguides should be smoothed cautiously to prevent the transverse derivative term $\partial_x^2(1/n(x))$ singularity in Eq. (4). A variety of functions were used [3,4, 9–11] to approximate such step-like refractive index profiles.

3. Smoothing functions

3.1. The sigmoid function

Historically, the first function suggested to smooth the refractive index profile was sigmoid and presented by Hoekstra et al. [12] and Yamauchi et al. [14]. The later pointed out that the choice of the steepness parameter in the sigmoid function is very sensitive in concern with power conservation [14]. Obviously, the second term in Eq. (4) can be written as:

$$\frac{n(x)}{k_o^2} \frac{\partial^2}{\partial x^2}\left(\frac{1}{n(x)}\right) = \frac{1}{k_0^2}\left\{-\frac{1}{n(x)} \frac{\partial^2 n(x)}{\partial x^2} + 2\left[\frac{1}{n(x)} \frac{\partial n(x)}{\partial x}\right]^2\right\} \quad (5)$$

The basic sigmoid function takes the form:

$$n_{sig} = \frac{1}{1 + e^{-a(x-x_o)}} \quad (6)$$

where, *a* is the steepness parameter which plays a vital role in the numerical stability of the calculations. The first and second derivatives of the sigmoid function with respect to *x* can be written as:

$$\partial_{xx}(n_{sig}) = \frac{e^{-a(x-x_o)}}{1 + e^{-a(x-x_o)}} = n_{sig}(1 - n_{sig}) \quad (7)$$

$$\partial_x^2(n_{sig}) = (\partial_x(n_{sig}))(1 - 2n_{sig}) \quad (8)$$

Substituting by Eqs. (7) and (8) into Eq. (5) and simplifying yields:

$$\frac{n_{sig}(x)}{k_o^2} \frac{\partial^2}{\partial x^2}\left(\frac{1}{n_{sig}(x)}\right) = \frac{1}{k_0^2}\{n_{sig} - 1\} \quad (9)$$

Finally, the equivalent refractive index takes the form:

$$n_{eq}^2 = n_{sig}^2 - \frac{1}{k_0^2}\{n_{sig} - 1\} \quad (10)$$

From this equation, the sigmoid function is stable as the right side is always positive, i.e. $n_{sig}^2 > n_{sig} - 1/k_0^2$. Fig. 1 shows the sigmoid function that approximates the step-index waveguide with air core ($n_{co} = 1$), silver cladding ($n_{cl} = 0.3970$ -*j*11.4) and width $w_p = 50$ nm. The smoothed index profile of such waveguide takes the form:

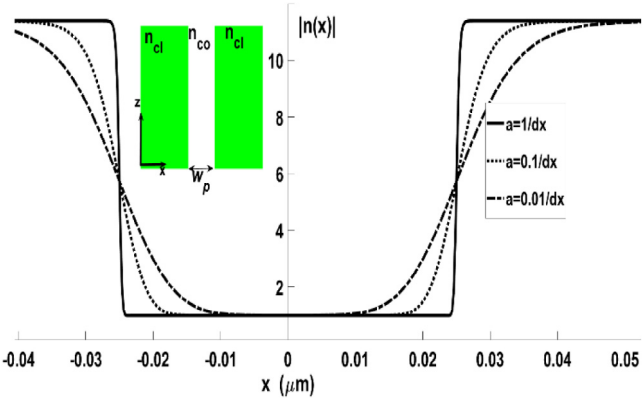

Fig. 1. The sigmoid function with different '*a*' value.

$$n_{sig}(x) = n_{cl} - \frac{\Delta n_1}{1 + e^{-a(x-w_p/2)}} + \frac{\Delta n_1}{1 + e^{-a(x+w_p/2)}},\ \Delta n_1 = n_{co} - n_{cl}, a = 1/\Delta x \quad (11)$$

Where Δx is the transverse sampling step size. In Fig. 1, the steepness parameter '*a*' is varied to show its effect on the slope of the smoothed index profile at the core-cladding interface. As the value of '$a \times \Delta x$' decreases, the function becomes smoother. Fig. 1 depicts the waveguide with Δx =22 nm.

3.2. The arctangent function

The arctangent smoothing function has been presented for the first time in a study of the Goos–Hänchen shift in TM polarization [9,11]. The step-like index profile at $x = 0$ is thus approximated by:

$$n_{arc}(x) = n_2 + \{\delta n[0.5 + \frac{\tan^{-1}(x/a)}{\pi}]\} \quad (12)$$

Where n_2 is the ambient (low-index) medium, '*a*' is the steepness parameter which can take on small values compared to the transverse sampling step size Δx. It describes the steepness of the transition of *n(x)* from n_2 in $x < 0$ to $(n_2 + \delta n) = n_1$ in $x \geq 0$. This is obvious, since as $a \to 0$, the $n_{arc}(x)$ tends to a sharp step change from n_1 for $x \geq 0$ to n_2 for $x < 0$. Inserting Eq. (12) in Eq. (4) we get the equivalent index profile n_{eq}^2 as:

$$n_{eq}^2(x) = n_{arc}^2 - \frac{n_{arc}(x)}{k_0^2}\left[\frac{2(\delta n)^2}{n_{arc}^3(x).\pi^2 a^2.(1 + \frac{x^2}{a^2})^2} + \frac{2x\delta n}{n_{arc}^2(x).\pi a^3.(1 + \frac{x^2}{a^2})^2}\right] \quad (13)$$

Fig. 2 depicts the arctangent function in a waveguide with the same parameters as in the sigmoid function case. Thus, the smoothing function takes the form:

$$n_{arc}(x) = n_1 + \Delta n_1[0.5 - \frac{\tan^{-1}((x - w_p/2)/a)}{\pi}] + \Delta n_2[-0.5 + \frac{\tan^{-1}((x + w_p/2)/a)}{\pi}] \quad (14)$$

The steepness parameter '*a*' is varied to show the steepness of the core boundaries. '*a*' is normalized to $1/\Delta x$ value, as the product '$a/\Delta x$'

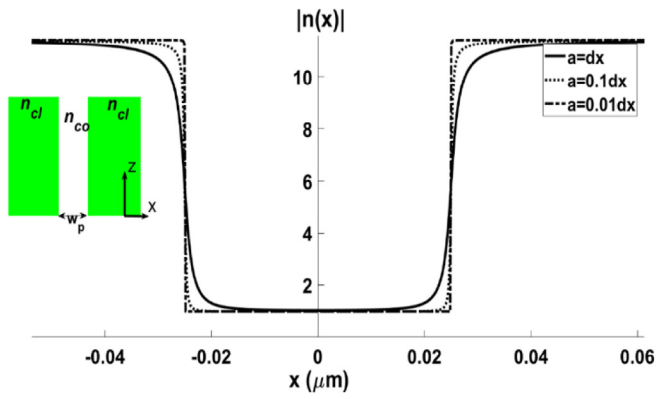

Fig. 2. The arctangent function with different '*a*' value.

decreases, the function becomes steeper in contrary to the sigmoid smoothing function.

3.3. The star function

we adopted the Smooth Transition Autoregressive (STAR) function [4] to approximate the refractive step-index profile $n_{pa}(x)$. Accordingly, the STAR function assumes the following form:

$$n_{pa}(x) = n_m + \frac{n_m e^{-(aW_p/2)} + n_d e^{ax}}{e^{-(aW_p/2)} + e^{ax}} - \frac{n_m e^{(aW_p/2)} + n_d e^{ax}}{e^{(aW_p/2)} + e^{ax}} \quad (15)$$

where, 'a' is the parameter (its unit is the inverse of the unit of x) that describes the steepness of the function n_{pa}. Fig. 3, depicts the smoothed profile $n_{pa}(x)$ for different values of 'a'.

3.4. The flat-top function

To the best of our knowledge, the flat-top (super-Gaussian) smoothing function is presented for the first time to approximate the refractive step-index profile of a step-index waveguide. Accordingly, the $n_{ft}(x)$ function assumes the following form:

$$n_{ft}(x) = n_{cl} + \Delta n e^{(x/w_p)^{2n}} \quad (16)$$

Where, n = 1,2,3.., and $\Delta n = n_{co} - n_{cl}$. Fig. 4 illustrates the flat-top smoothing function that approximates the step-index profile of the waveguide considered in the previous sections.

Evidently, as 'n' increases the function tends to be an abrupt step that changes from n_{co} to $n_{co}+\Delta n$.

4. Comparison between smoothing functions: stability and power conservation

4.1. Equivalent refractive index:

Fig. 5 shows the refractive index profile of a waveguide with w_p=300 nm, n_{co} = 3.477, and n_{cl} = 1. Using different smoothing functions and the parameters summarized in Table 1. We shall consider the guided mode power to assess the effect of the different smoothing functions on the stability of calculations. Fig. 6 depicts the numerical spikes at the boundaries (core/cladding interface and core/substrate interface) due to the second derivative of $(1/n(x))$. These numerical artifacts produce erroneous profile as in the case of star function, or fictitious complex values of the equivalent index, which result in an attenuated or amplified field in dielectric (lossless) waveguides.

Whilst, the sigmoid function is smooth at the boundaries without numerical spikes, due to the beneficial exact recurrence relation as derived in Eq. (10).

Table 1
The summary of the steepness parameters for the different smoothing functions.

The smoothing function	The steepness parameter
Sigmoid	a=2/dx
Arctan	a=0.25dx
Star	a=1/dx
Flat-top	*n=2*

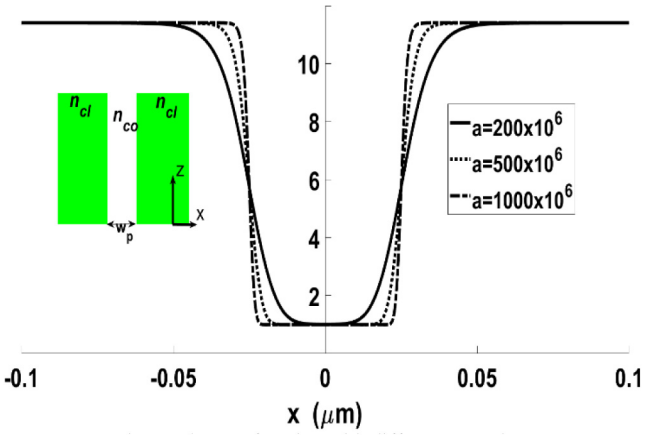

Fig. 3. The star function with different 'a' value.

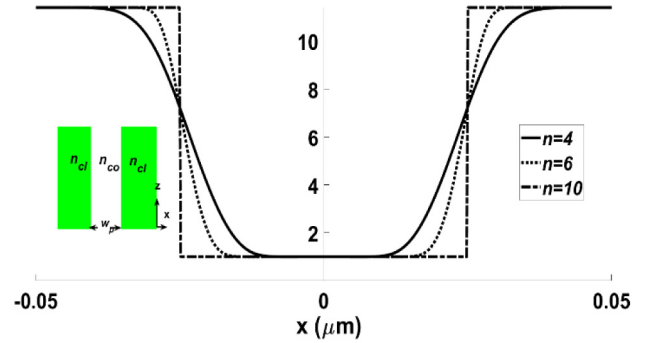

Fig. 4. The flat-top function with different 'n' value.

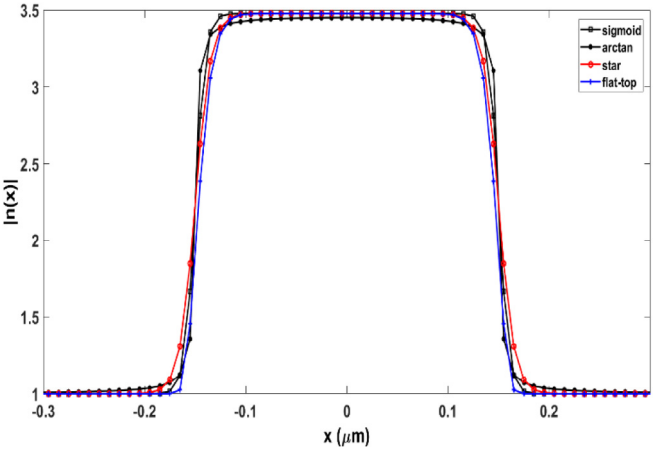

Fig. 5. The absolute refractive index profile |n(x)| for different smoothing functions with at 'a' value.

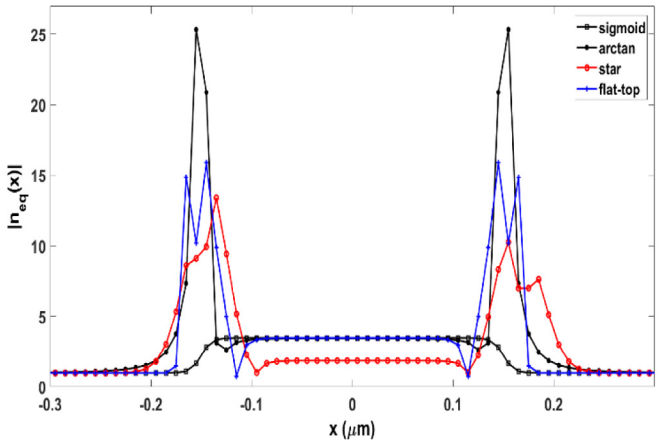

Fig. 6. The equivalent refractive index profile $n_{eq}(x)$ for different smoothing functions.

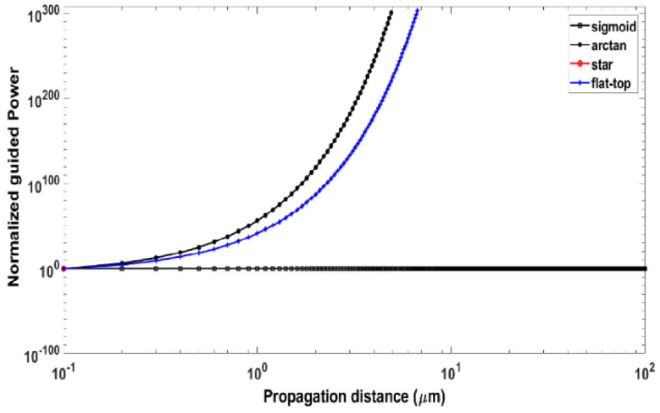

Fig. 7. The normalized guided power of different refractive index profiles $n_{eq}(x)$ for different smoothing functions.

4.2. Power stability

The second important characteristic of smoothing functions is the propagated power of TM mode, which must be stable [8,13]. Fig. 7 depicts the normalized propagated power in a dielectric waveguide. As shown, the sigmoid function with the equivalent refractive index calculated from Eq. (10) is stable. However, the other functions are not stable beyond some short propagation distance. The numerical evaluation of $\partial^2(1/n(x))/\partial x^2$ around the core boundaries generates an accumulated erroneous built-up field $\partial^2(1/n(x))/\partial x^2$ [14] while some steepness parameter values result in a complex equivalent index. Consequently, the argument of the phase correction operator of the BPM framework becomes complex i.e.:

$$Q_x = \exp\{-j\Delta z k_0(n_{eq} - n_o)\}$$
$$= \exp\{-j\Delta z k_0(real(n_{eq}) - n_o)\}\exp\{\pm\Delta z k_0(imag(n_{eq}) - n_o)\} \quad (17)$$

Hence, the propagated power is amplified (or attenuated) erroneously. Evidently, the STAR function starts to upswing from the beginning (not shown in the figure) as the STAR function is very sensitive to the steepness parameter relative to the other functions.

5. Numerical results

5.1. Waveguide facet

For comparison, a dielectric waveguide terminated by air were studied using a TM polarization mode. The inset of Fig. 8, depicts

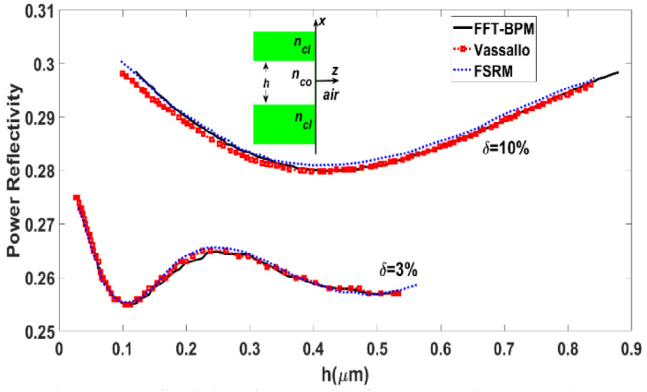

Fig. 8. The power reflectivity of waveguide facet comparison curve between FSRM [17], Vassallo [16], and proposed FFT-BPM method.

the geometry of the problem under consideration where a three-layer dielectric slab waveguide occupying the half-space $z<0$ is abruptly terminated by air at $z = 0$. As shown, $n_{co} = 3.6$ is the waveguide core refractive index and its width h varies from 1~900 nm, and surrounded by a symmetric cladding of refractive index $n_{cl} = n_{co}(1-\delta)$. The power reflectivity is calculated [15] where $\delta = 3\%$, and 10%, and the free space wavelength $\lambda_o = 0.86$ μm. As shown in Fig. 8 the power reflectivity compared with Vassallo [16] and FSRM [17], the curves reveal a general good agreement between the proposed method and other methods.

5.2. Plasmon mode excitation in MIM waveguide

As a test of the method, we consider a metal dielectric metal (MIM) waveguide with $W_p = 50$ nm (single mode at wavelength 1.55 μm) excited, at z=0, with a y-polarized Gaussian beam having a full 1/e width $W_G = 250$ nm. Fig. 9(a) depicts a 3-D plot of the field from $z = 0$ to $z = 20$ nm. In the immediate vicinity of the incidence plane $z = 0$, the plasmonic mode profile is well established after few nanometers, and Fig. 9(b) shows the color contour plot corresponding to Fig. 9(a).

5.3. Plasmon mode excitation in Kretschmann configuration

An extremely narrow subwavelength rectangular pulse is used for the efficient resonant excitation of the TM_0mode as shown in the inset of Fig. 10(a). The waveguide is made of asymmetric layers: glass–silver–air (Kretschmann configuration). The pulse is incident at the resonance angle corresponding to surface plasmon TM_0 mode. The parameters as following:

The parameter	The value	The parameter	The value
The sampling interval Δx	0.5 nm	The step size Δz	0.5 Δx
The resonance angle θ_p	42.26°	The glass index of refraction ng	1.5
The refractive index of silver	0.157-*j*4	The light wavelength	0.633 μm
The total propagation distance	430 nm	The total number of sampling points along the x-direction N	215
The pulse width W_r	100 nm	The plasmon guide width W_p	100 nm

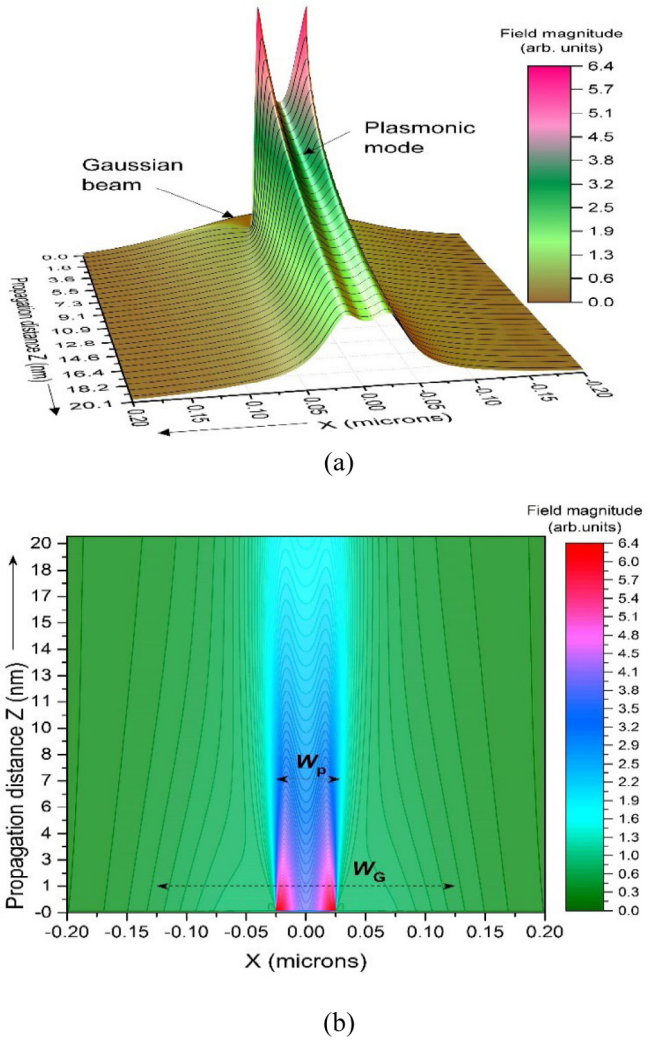

Fig. 9. (a) Gaussian beam incident on a MIM waveguide at z=0. The fundamental mode profile TM_0 is rapidly established few nanometers away from the incidence plane. (b) Strong light-confinement within the core of the MIM guide during the establishment of the modal field of the guide.

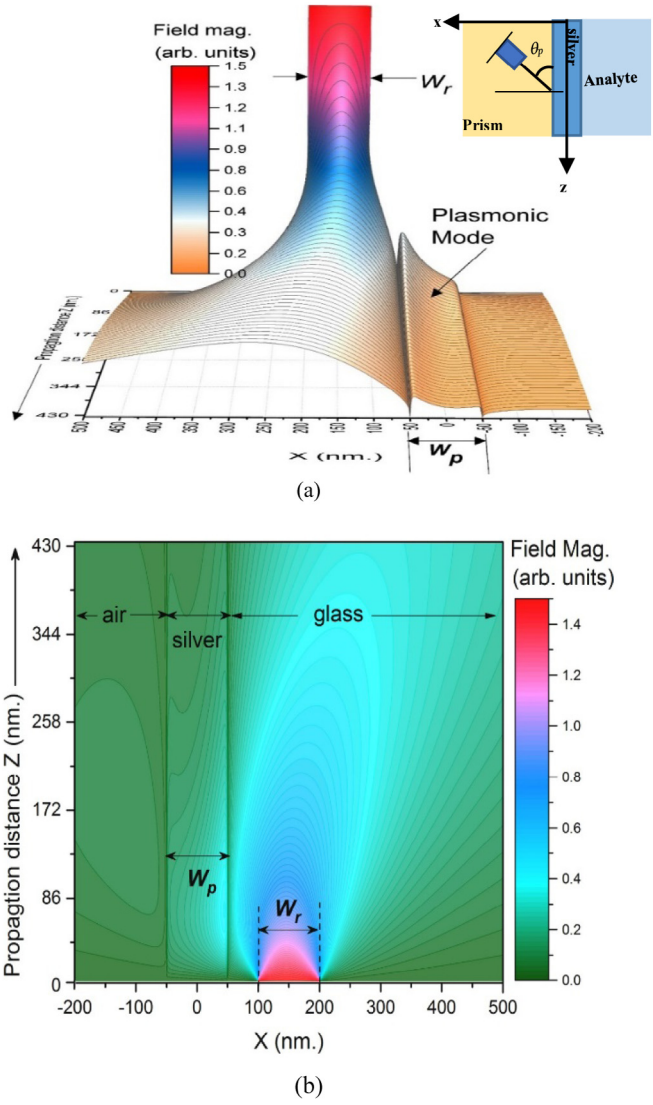

Fig. 10. Excitation of the TM_0 mode of the plasmonic guide by a subwavelength narrow rectangular pulse. The pulse width and the silver film thickness are equal to 100 nm.

The plane wave component in the angular spectrum of the rectangular pulse corresponding to that resonance has a k_{xp} value equal to $k_0 n_g cos\theta_p = 10.82\ \mu m^{-1}$; this corresponds to a k_{zp} component $k_0 n_g sin\theta_p = 10.34\ \mu m^{-1}$. This component should be equal to the real part (β_r) of the complex propagation constant of the TM_0 mode. The numerical solution of the eigenvalue equation of that mode of the insulator metal insulator (IMI) waveguide [18], gives an effective index $n_{eff} = \beta_r / k_0 = 1.031$, which agrees with the value $k_{zp}/k_0 = 1.036$. The rapid growth of the fundamental plasmonic mode is depicted in Fig. 10 b, which shows the evolution of the magnetic field along the propagation direction z.

To test the proper behavior of the evanescent waves associated with the excitation problem, a deeper consideration of these types of waves is needed. The angular spectrum of these evanescent waves has k_x values greater than $k_0 n_0$ (where n_0 is the reference refractive index of the homogeneous medium used in the BPM algorithm). Accordingly, the longitudinal component k_z of the wave vector corresponding to this range ($k_x > k_0 n_0$) is written as [19]:

$$k_z = \sqrt{k_o^2 n_o^2 - k_x^2} = -j\sqrt{k_x^2 - k_o^2 n_o^2} \tag{18}$$

Hence, the evanescent waves decay along the propagation direction since the phase factor varies over the propagation step Δz as:

$$e^{-jk_z \Delta z} = e^{-\Delta z \sqrt{k_x^2 - k_o^2 n_o^2}} \tag{19}$$

Thus, the inhomogeneous field K^i of the evanescent waves contributes to the total propagated field during the propagation step Δz via a decaying part of the form [19]:

$$K^i(x,z) = \frac{1}{2\pi} \int_{|k_x| > k_o n_o} k(k_x) e^{jk_x x} e^{-\Delta z \sqrt{k_x^2 - k_o^2 n_o^2}} dk_x \tag{20}$$

This guarantees the proper decay of the evanescent waves in the propagation direction. Fig. 11(a), depicts the magnitude of $K^i(x,z)$ along the propagation direction z. The fast decay of that field is noticeable as well in the contour plot Fig. 11(b).

5.4. Plasmon waveguide facet

Fig. 12 shows the power reflectivity (a) and power transmissivity (b) of MIM waveguide coated with a single dielectric layer, as function of the coating layer thickness. The coating layer thickness is varied

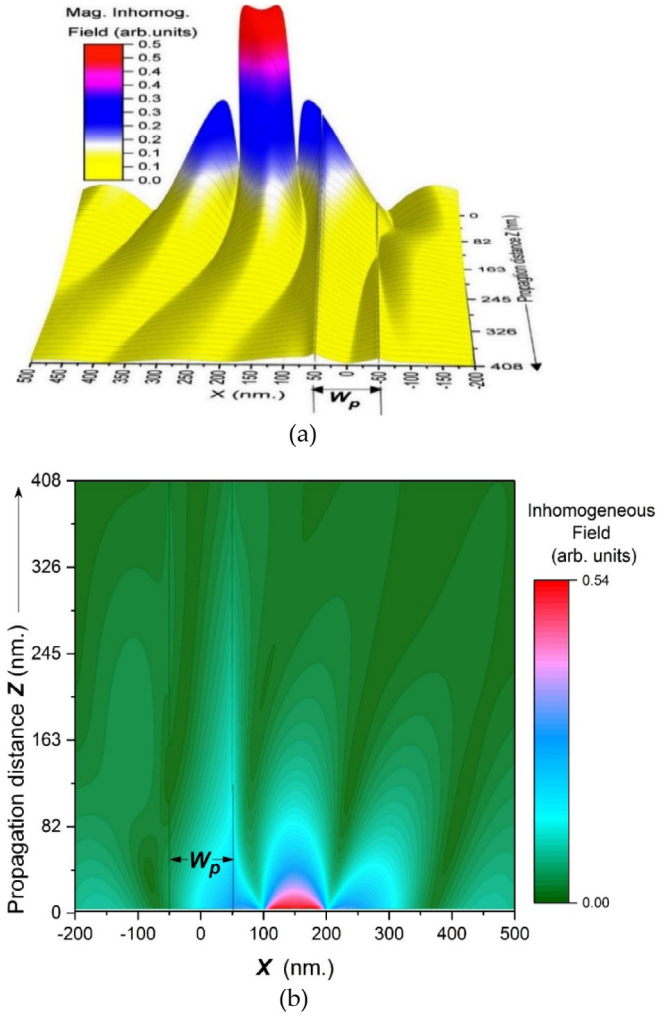

Fig. 11. Evolution of the inhomogeneous component K^i of the total field when a rectangular subwavelength pulse excites the fundamental mode TM_0 of the plasmonic guide as shown in the inset of Fig. 10(a). The pulse has the same width (100 nm) as the core of the plasmonic guide.

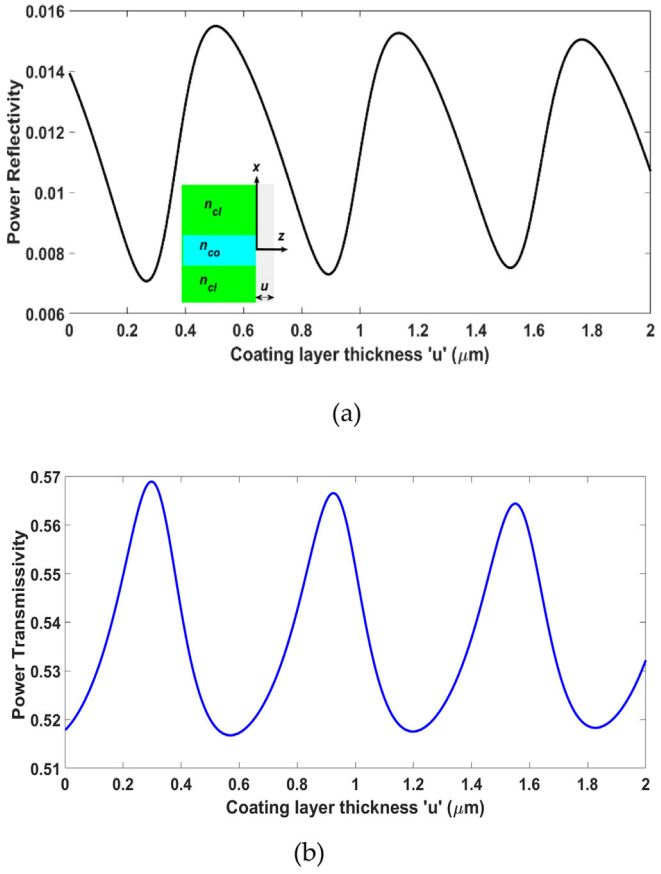

Fig. 12. The power reflectivity (a) and power transmissivity (b) of MDM waveguide coated with single dielectric material as function of the coating layer thickness.

from 1 to 800 nm. The MIM waveguide core refractive index n_{co} = 1.515, the metal cladding refractive index n_{cl} = 0.397018 - j11.9856. The fundamental modal field is calculated by solving numerically the corresponding eigenvalue equations [18]. Whilst β_p is the propagation constant of the TM_0 mode of the plasmonic waveguide, hence, the plasmonic mode effective index$n_e = (\beta_p/k_0)$. The coating layer has an index equal to the square root of the "*real part*" of the plasmonic mode effective index *real*(n_e), which is equal to 1.230598 at a wavelength λ_o = 1.55 μm. Theoretically, the oscillation in the power reflectivity and power transmissivity are akin of the well-known response of a Fabry–Perot resonator [20–22]. Fig. 12 a and b depict a periodicity of the order $\lambda/[2\times real(n_e)]\approx 0.59$ μm.

6. Conclusion

Classical FFT-BPM could not deal with plasmonic and subwavelength structure which is a TM problem in nature. So, different smoothing functions are investigated to convert the TM problem to an equivalent TE one. A variety of subwavelength structures have been presented and studied. We claim that a judiciously chosen smoothing function will render the traditional FFT-BPM more versatile to consider nano scale waveguiding structures involving metals and dielectrics. This will be very useful to the computational and assessment of many complicated subwavelength nanostructures.

CRediT authorship contribution statement

Adel Shaaban: Calculations, Writing. **Yi-Chun Du:** Writing - review & editing. **Lotfy Rabeh Gomaa:** Calculations, Writing.

Declaration of competing interest

The authors declare that they have no known competing financial interests or personal relationships that could have appeared to influence the work reported in this paper.

Acknowledgments

The authors would like to thank the support from the National Center for Radiation Research (NCRRT) at Atomic Energy Authority in Egypt.

All authors read and approved the final manuscript.

Funding

This research was funded by the Ministry of Science and Technology, Taiwan (MOST 108-2221-E-218-005-MY3).

References

[1] E.-P. Li, H.-S. Chu, Plasmonic Nanoelectronics and Sensing, Cambridge university press, 2014.

[2] S. Zouhdi, A. Sihvola, A.P. Vinogradov, Metamaterials and Plasmonics: Fundamentals, Modelling, Applications, Springer Science & Business Media, 2008.

[3] A. Shaaban, Y.-C. Du, L.R. Gomaa, Extension of an FFT-based beam propagation method to plasmonic and dielectric waveguide discontinuities and junctions, Appl. Sci. 9 (20) (2019) 4362.
[4] A. Shaaban, Y.-C. Du, L.R. Gomaa, Transmissivity assessment of plasmonic-dielectric waveguide interconnects via modified FFT-BPM, Optik (2019) 164143.
[5] L. Nickelson, Electromagnetic Theory and Plasmonics for Engineers, 2019.
[6] A.R. Zakharian, J.V. Moloney, M. Mansuripur, Surface plasmon polaritons on metallic surfaces, Opt. Express 15 (1) (2007) 183–197.
[7] Z. Zang, K. Mukai, P. Navaretti, M. Duelk, C. Velez, K. Hamamoto, Thermal resistance reduction in high power superluminescent diodes by using active multi-mode interferometer, Appl. Phys. Lett. 100 (3) (2012) 31108.
[8] Sükrü Ekin Kocabacs, G. Veronis, D.A.B. Miller, S. Fan, Modal analysis and coupling in metal–insulator–metal waveguides, Phys. Rev. B 79 (3) (2009) 35120.
[9] C. Vassallo, Difficulty with vectorial BPM, Electron. Lett. 33 (1) (1997) 61–62.
[10] L.R. Gomaa, A. Shaaban, M.F.O. Hameed, S.S.A. Obayya, Competitiveness of the BPM in studying the optical beams at critical incidence on dielectric interfaces, Opt. Quantum Electron. 49 (2) (2017) http://dx.doi.org/10.1007/s11082-016-0886-2.
[11] A. Shaaban, Y.-C. Du, L. Gomaa, Integrated sensitive biosensor with surface plasmon for dengue fever detection, in: 2020 IEEE 8th International Conference on Photonics (ICP) (ICP2020), 2020.
[12] H. Hoekstra, et al., A cost 240 benchmark test for beam propagation methods applied to an electrooptical modulator based on surface plasmons, J. Lightwave Technol. 16 (10) (1998) 1921.
[13] L. Poladian, F. Ladouceur, Unification of TE and TM beam propagation algorithms, IEEE Photonics Technol. Lett. 10 (1) (1998) 105–107.
[14] J. Yamauchi, N. Shimada, Y. Nito, H. Nakano, Transverse-magnetic BPM analysis of a step-index slab waveguide expressed by a sigmoid function, IEEE Photonics Technol. Lett. 21 (3) (2008) 149–151.
[15] A. Shaaban, Y.-C. Du, L.R. Gomaa, Extension of an FFT-based beam propagation method to plasmonic and dielectric waveguide discontinuities and junctions, Appl. Sci. 9 (20) (2019) http://dx.doi.org/10.3390/app9204362.
[16] C. Vassallo, Reflectivity of multidielectric coatings deposited on the end facet of a weakly guiding dielectric slab waveguide, J. Opt. Soc. Amer. A 5 (11) (1988) 1918–1928.
[17] C.J. Smartt, T.M. Benson, P.C. Kendall, 'free space radiation mode'method for the analysis of propagation in optical waveguide devices, IEE Proc. J 140 (1) (1993) 56–61.
[18] J. Orfanidis Sophocles, Electromagnetic Waves and Antennas, 2003.
[19] M.W. Kowarz, Homogeneous and evanescent contributions in scalar near-field diffraction, Appl. Opt. 34 (17) (1995) 3055–3063.
[20] A. Shaaban, M.F.O. Hameed, L.R. Gomaa, S.S.A. Obayya, Accurate calculation of Goos-Hänchen shift at critical angle for complex laser beam profiles using beam propagation method, Optik 157 (2018) 1106–1114.
[21] G. Veronis, S. Fan, Theoretical investigation of compact couplers between dielectric slab waveguides and two-dimensional metal–dielectric-metal plasmonic waveguides, Opt. Express 15 (3) (2007) 1211–1221.
[22] A. Shaaban, Hybrid Plasmonic-Dielectric Guiding Structures for Interfacing and Sensing, 2020.